

June 4, 2022

Open charm spectroscopy at LHCb

MARK WHITEHEAD¹

*Department of Physics
University of Warwick, Coventry, CV4 7AL, UK*

Recent charm spectroscopy results from Dalitz plot analyses of B decays to open charm final states at LHCb are presented. The decay modes used are $B^+ \rightarrow D^- K^+ \pi^+$, $B^0 \rightarrow \bar{D}^0 \pi^+ \pi^-$ and $B^0 \rightarrow \bar{D}^0 K^+ \pi^-$.

PRESENTED AT

The 7th International Workshop on Charm Physics
(CHARM 2015)
Detroit, MI, 18-22 May, 2015

¹Work supported by the European Research Council.

1 Introduction

The family of charm mesons are predicted by heavy quark effective theory [1] and lattice QCD [2]. The 1P states have been well measured by the B -factories and LHCb [3, 4, 5, 6]. Evidence for higher mass $D(2600)$ and $D(2760)$ states has been seen [5, 6]. Only natural spin-parity resonances ($J^P = 0^+, 1^-, 2^+, \dots$) contribute in $B \rightarrow D_{(s)}hh'$ decays where h and h' are kaons and pions. In 2014 LHCb published results from a Dalitz plot analysis of $B_s^0 \rightarrow \bar{D}^0 K^- \pi^+$ decays, which included the first observation of the $D_{s1}(2860)^-$ and $D_{s3}(2860)^-$ mesons [7, 8]. These states are thought to be members of the D_s 1D family [9, 10]. It is therefore interesting to explore D meson spectroscopy to find and identify new states to compare their properties with the theory predictions. Three analyses are presented, using $B^+ \rightarrow D^- K^+ \pi^+$ [11], $B^0 \rightarrow \bar{D}^0 \pi^+ \pi^-$ [12] and $B^0 \rightarrow \bar{D}^0 K^+ \pi^-$ decays [13].

2 Dalitz plot analysis of $B^+ \rightarrow D^- K^+ \pi^+$ decays

The first observation of the decay $B^+ \rightarrow D^- K^+ \pi^+$, with $D^- \rightarrow K^+ \pi^- \pi^-$, is made using the topologically similar decay $B^+ \rightarrow D^- \pi^+ \pi^+$ as a normalisation channel [11]. Event selection is based on a neural network used to reduce combinatorial background. Candidates in the signal and normalisation channels are shown in Fig. 1, with fits used to extract the signal and normalisation channel yields overlaid. Accounting for the selection efficiencies gives the branching fraction ratio

$$\frac{\mathcal{B}(B^+ \rightarrow D^- K^+ \pi^+)}{\mathcal{B}(B^+ \rightarrow D^- \pi^+ \pi^+)} = 0.0720 \pm 0.0019 \pm 0.0021, \quad (1)$$

where the uncertainties are statistical and systematic, respectively. Using the known value of $\mathcal{B}(B^+ \rightarrow D^- \pi^+ \pi^+) = (1.01 \pm 0.05) \times 10^{-3}$ [14] gives

$$\mathcal{B}(B^+ \rightarrow D^- K^+ \pi^+) = (7.31 \pm 0.19 \pm 0.22 \pm 0.39) \times 10^{-5}, \quad (2)$$

where the third uncertainty is from $\mathcal{B}(B^+ \rightarrow D^- \pi^+ \pi^+)$.

The Dalitz plot analysis is performed on candidates in the B mass window 5239.4–5317.1 MeV (natural units are used throughout), with about 2000 signal candidates and a purity of approximately 93%. In $B^+ \rightarrow D^- K^+ \pi^+$ decays, resonances are only expected to appear in $m(D\pi)$, allowing angular moments from the Legendre polynomials to be used to guide the amplitude model. The moments study showed no evidence of structures above spin 2. The components included in the amplitude model are shown in Table 1.

The amplitude fit is performed with the Laura++ package [15] using the isobar formalism [16, 17, 18], with histograms to describe backgrounds and signal efficiency.

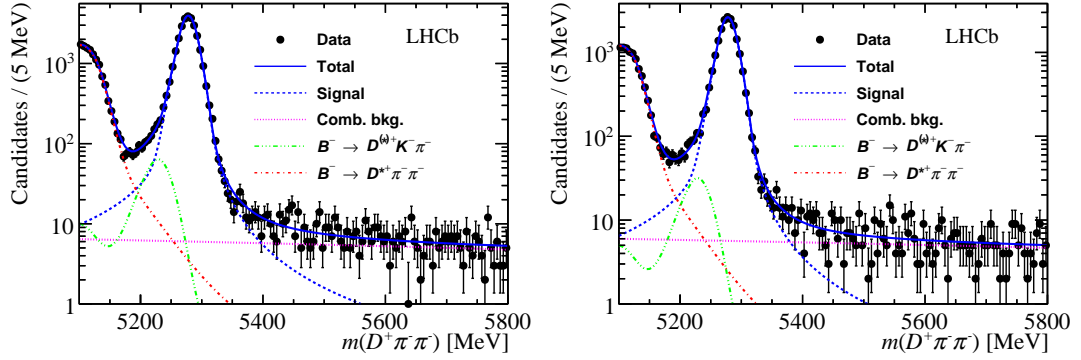


Figure 1: Fits to the B candidate invariant mass distribution for (left) $B^+ \rightarrow D^- \pi^+ \pi^+$ and (right) $B^+ \rightarrow D^- K^+ \pi^+$ candidates. Components are described in the legend.

Resonance	Spin	DP axis	Model	Parameters
$D_0^*(2400)^0$	0	$m^2(D\pi)$	RBW	$m = 2318 \pm 29\text{MeV}, \Gamma = 267 \pm 40\text{MeV}$
$D_2^*(2460)^0$	2	$m^2(D\pi)$	RBW	Determined from data
$D_J^*(2760)^0$	1	$m^2(D\pi)$	RBW	Determined from data
Nonresonant	0	$m^2(D\pi)$	EFF	Determined from data
Nonresonant	1	$m^2(D\pi)$	EFF	Determined from data
$D_v^*(2007)^0$	1	$m^2(D\pi)$	RBW	$m = 2006.98 \pm 0.15\text{MeV}, \Gamma = 2.1\text{MeV}$
B_v^{*0}	1	$m^2(DK)$	RBW	$m = 5325.2 \pm 0.4\text{MeV}, \Gamma = 0.0\text{MeV}$

Table 1: Components of the $B^+ \rightarrow D^- K^+ \pi^+$ amplitude fit model. RBW and EFF are the relativistic Breit-Wigner function and exponential form factor, respectively. Terms with subscript v are virtual components, where the resonant pole mass is outside of the Dalitz plot boundary.

For the full fit results see Ref. [11]. Figure 2 shows the fit projection in $m(D\pi)$. Significant contributions are seen from the $D_0^*(2400)^0$, $D_2^*(2460)^0$ and $D_J^*(2760)^0$ states, where the spin of the latter is determined to be 1 for the first time. Other spin hypotheses are rejected with high significance ($> 6\sigma$). The mass and width for the $D_1^*(2760)^0$ and $D_2^*(2460)^0$ resonances are found to be

$$\begin{aligned}
m(D_2^*(2460)^0) &= (2464.0 \pm 1.4 \pm 0.5 \pm 0.2) \text{ MeV}, \\
\Gamma(D_2^*(2460)^0) &= (43.8 \pm 2.9 \pm 1.7 \pm 0.6) \text{ MeV}, \\
m(D_1^*(2760)^0) &= (2781 \pm 18 \pm 11 \pm 6) \text{ MeV}, \\
\Gamma(D_1^*(2760)^0) &= (177 \pm 32 \pm 20 \pm 7) \text{ MeV},
\end{aligned}$$

where the uncertainties are statistical, experimental systematic and model dependent systematic, respectively.

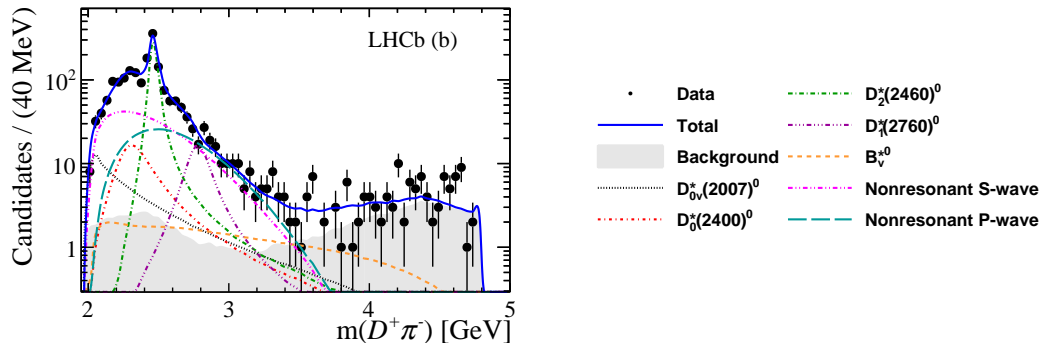


Figure 2: Projection of the amplitude fit in $m(D\pi)$ for $B^+ \rightarrow D^- K^+ \pi^+$ candidates. Components are as described in the legend.

3 Dalitz plot analysis of $B^0 \rightarrow \bar{D}^0 \pi^+ \pi^-$ decays

The amplitude analysis of the $B^0 \rightarrow \bar{D}^0 \pi^+ \pi^-$ final state is performed using the $\bar{D}^0 \rightarrow K^+ \pi^-$ decay [12]. With larger data samples this channel can be used to measure $\cos(2\beta)$ and $\sin(2\beta)$ [19, 20], where β is an angle of the unitarity triangle. Resonant structures are expected in both $m(D\pi)$ and $m(\pi\pi)$. Combinatorial background is removed using a Fisher discriminant multivariate selection. Figure 3 shows the B candidate invariant mass distribution of selected candidates. The signal window used in the amplitude analysis is 5250–5310 MeV. It contains about 10000 signal candidates with a signal purity of around 98 %.

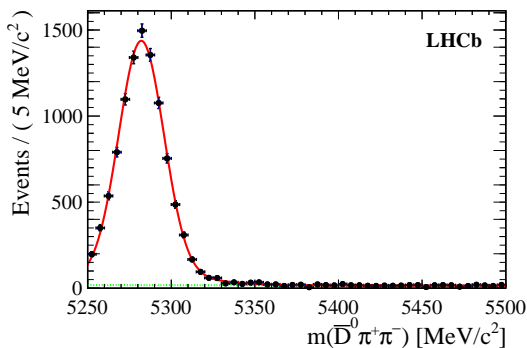


Figure 3: Fit to the B candidate invariant mass distribution for $B^0 \rightarrow \bar{D}^0 \pi^+ \pi^-$ decays. The data are black points and the fit and backgrounds are shown in red and green, respectively.

Two amplitude fits are performed, using the isobar model and a K-matrix approach [21, 22] for the $\pi\pi$ S-wave contribution. The resonances included in the models are shown in Table 2. Projections of the isobar model fit are shown in Fig 4, see Ref. [12] for the K-matrix results. The charm resonances $D_0^*(2400)^-$, $D_2^*(2460)^-$

and $D_j^*(2760)^-$ are found to be significant and the $D_j^*(2760)^-$ state is determined, with high significance, to be spin 3 for the first time. It is interesting to note that in the $B^+ \rightarrow D^- K^+ \pi^+$ analysis the $D_j^*(2760)^0$ was found to be spin 1. This suggests that there could be two overlapping states, as was seen in the D_s meson family in $B_s^0 \rightarrow \bar{D}^0 K^- \pi^+$ decays [7, 8]. The masses and widths of the charm resonances from the isobar model fit are

$$\begin{aligned}
m(D_0^*(2400)^-) &= (2349 \pm 6 \pm 1 \pm 4) \text{ MeV}, \\
\Gamma(D_0^*(2400)^-) &= (217 \pm 13 \pm 5 \pm 12) \text{ MeV}, \\
m(D_2^*(2460)^-) &= (2468.6 \pm 0.6 \pm 0.0 \pm 0.3) \text{ MeV}, \\
\Gamma(D_2^*(2460)^-) &= (47.3 \pm 1.5 \pm 0.3 \pm 0.6) \text{ MeV}, \\
m(D_3^*(2760)^-) &= (2798 \pm 7 \pm 1 \pm 7) \text{ MeV}, \\
\Gamma(D_3^*(2760)^-) &= (105 \pm 18 \pm 6 \pm 23) \text{ MeV},
\end{aligned}$$

where the uncertainties are statistical, experimental systematic and model dependent systematic, respectively. Good agreement is seen between the isobar model and K-matrix fit results.

Resonance	Spin	Model	m_r (MeV)	Γ_0 (MeV)
$D^0 \pi^-$ P-wave	1	[12]		Floated
$D_0^*(2400)^-$	0	RBW		Floated
$D_2^*(2460)^-$	2	RBW		Floated
$D_j^*(2760)^-$	3	RBW		Floated
$\rho(770)$	1	GS	775.02 ± 0.35	149.59 ± 0.67
$\omega(782)$	1	[12]	781.91 ± 0.24	8.13 ± 0.45
$\rho(1450)$	1	GS	1493 ± 15	427 ± 31
$\rho(1700)$	1	GS	1861 ± 17	316 ± 26
$f_2(1270)$	2	RBW	1275.1 ± 1.2	$185.1^{+2.9}_{-2.4}$
$\pi\pi$ S-wave	0	K-matrix		[12]
$f_0(500)$	0	[12]		[12]
$f_0(980)$	0	FLT		[12]
$f_0(2020)$	0	RBW	1992 ± 16	442 ± 60
Nonresonant	0	[12]		[12]

Table 2: Components of the isobar and K-matrix amplitude fit models to $B^0 \rightarrow \bar{D}^0 \pi^+ \pi^-$ decays. GS is the Gounaris-Sakurai function and FLT is the Flatté shape. See Ref. [12] for more details.

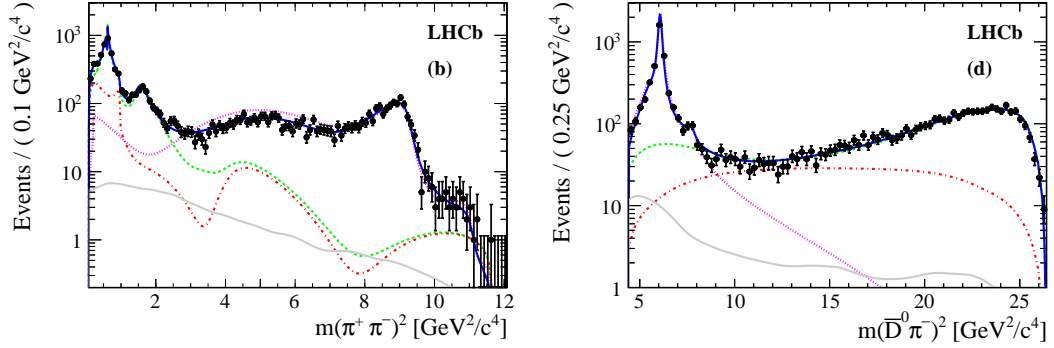


Figure 4: Projection of the isobar model fit in (left) $m(\pi\pi)$ and (right) $m(D\pi)$ for $B^0 \rightarrow \bar{D}^0\pi^+\pi^-$ candidates. The components are (black) data, (blue) isobar fit, (green) $\pi^+\pi^-$ P- and D-wave, (pink) $D\pi$ contributions, (red) $\pi^+\pi^-$ S-wave and (grey) background.

4 Dalitz plot analysis of $B^0 \rightarrow \bar{D}^0 K^+ \pi^-$ decays

An amplitude analysis of $B^0 \rightarrow \bar{D}^0 K^+ \pi^-$ decays with $\bar{D}^0 \rightarrow K^+ \pi^-$ is presented [13]. The goal of studying $B^0 \rightarrow DK^+ \pi^-$ decays is to measure the unitarity triangle angle γ , as outlined in Refs. [23, 24]. It can also be used to access the same charm resonances as $B^0 \rightarrow \bar{D}^0 \pi^+ \pi^-$ decays, although the available statistics are smaller. Contributions also appear in the $m^2(K\pi)$ axis of the Dalitz plot.

The event selection is based on a neural network to distinguish between signal and combinatorial background. The B candidate mass distribution of selected events is shown in Fig. 5, overlaid with the fit used to determine the signal and background yields. Events in the signal region, defined as 5248.6–5309.1 MeV, are selected for the Dalitz plot fit. There are approximately 2500 signal candidates with a purity of around 75% in this window.

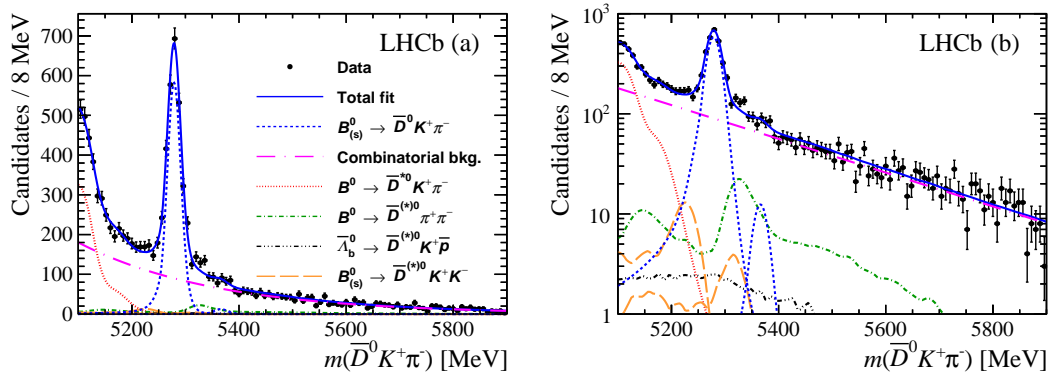


Figure 5: Fit to the B candidate invariant mass distribution for $B^0 \rightarrow \bar{D}^0 K^+ \pi^-$ candidates with (left) linear and (right) log y -axis scales. Components are described in the legend.

The amplitude fit contains contributions from the terms shown in Table 3 and is performed using the Laura++ package [15] with the isobar formalism. Backgrounds and efficiency corrections are both accounted for in the fit. For the full results of the amplitude fit see Ref. [13]. The projections of the amplitude fit in $m(D\pi)$ and $m(K\pi)$ are shown in Fig. 6 (left) and (right), respectively.

Resonance	Spin	DP axis	Model	Parameters (MeV)
$K^*(892)^0$	1	$m^2(K\pi)$	RBW	$m_0 = 895.81 \pm 0.19, \Gamma_0 = 47.4 \pm 0.6$
$K^*(1410)^0$	1	$m^2(K\pi)$	RBW	$m_0 = 1414 \pm 15, \Gamma_0 = 232 \pm 21$
$K_0^*(1430)^0$	0	$m^2(K\pi)$	LASS	Determined from data
$K_2^*(1430)^0$	2	$m^2(K\pi)$	RBW	$m_0 = 1432.4 \pm 1.3, \Gamma_0 = 109 \pm 5$
$D_0^*(2400)^-$	0	$m^2(D\pi)$	RBW	Determined from data
$D_2^*(2460)^-$	2	$m^2(D\pi)$	RBW	Determined from data
Nonresonant	0	$m^2(D\pi)$	dabba	Fixed
Nonresonant	1	$m^2(D\pi)$	EFF	Determined from data

Table 3: Components included in the $B^0 \rightarrow \bar{D}^0 K^+ \pi^-$ amplitude fit model. More details on the dabba and LASS models can be found in Ref. [13].

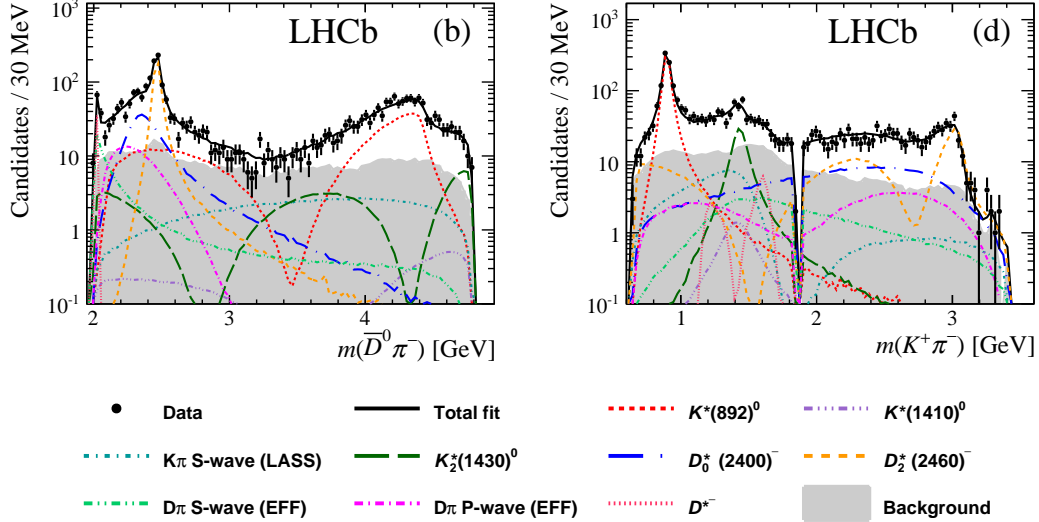


Figure 6: Projection of the amplitude fit in (left) $m(D\pi)$ and (right) $m(K\pi)$ for $B^0 \rightarrow \bar{D}^0 K^+ \pi^-$ candidates. Components are described in the legend. The dip in the right plot is due to a veto at $m(D^0)$.

The charm resonance results are in agreement with the $B^0 \rightarrow \bar{D}^0 \pi^+ \pi^-$ analysis. Due to the lower statistics available no contribution is seen at $m(D\pi) \approx 2760$ MeV.

The masses and widths of the states $D_0^*(2400)^-$ and $D_2^*(2460)^-$ are reported to be

$$\begin{aligned}
m(D_0^*(2400)^-) &= (2360 \pm 15 \pm 12 \pm 28) \text{ MeV}, \\
\Gamma(D_0^*(2400)^-) &= (255 \pm 26 \pm 20 \pm 47) \text{ MeV}, \\
m(D_2^*(2460)^-) &= (2465.6 \pm 1.8 \pm 0.5 \pm 1.2) \text{ MeV}, \\
\Gamma(D_2^*(2460)^-) &= (46.0 \pm 3.4 \pm 1.4 \pm 2.9) \text{ MeV},
\end{aligned}$$

where the uncertainties are statistical, experimental systematic and model dependent systematic, respectively. These results are in agreement with those from the $B^0 \rightarrow \bar{D}^0 \pi^+ \pi^-$ analysis but are less precise.

5 Summary

The latest results on charm spectroscopy from Dalitz plot analyses of B meson decays at LHCb are presented. First observations are made of the $D_1^*(2760)^0$ and $D_3^*(2760)^-$ mesons. Larger data samples are needed to determine whether or not the isospin partners of these states can be seen.

ACKNOWLEDGEMENTS

I thank the members of the LHCb collaboration for their help in preparing the talk and this document. Work supported by the European Research Council under FP7.

References

- [1] S. Godfrey and N. Isgur, Phys. Rev. D **32**, 189 (1985).
- [2] D. Mohler, S. Prelovsek and R. M. Woloshyn, Phys. Rev. D **87**, 034501 (2013)
- [3] K. Abe *et al.* [Belle Collaboration], Phys. Rev. D **69**, 112002 (2004)
- [4] B. Aubert *et al.* [BaBar Collaboration], Phys. Rev. D **79**, 112004 (2009)
- [5] P. del Amo Sanchez *et al.* [BaBar Collaboration], Phys. Rev. D **82**, 111101 (2010)
- [6] R. Aaij *et al.* [LHCb Collaboration], JHEP **109**, 145 (2013)
- [7] R. Aaij *et al.* [LHCb Collaboration], Phys. Rev. Lett. **113**, 162001 (2014)
- [8] R. Aaij *et al.* [LHCb Collaboration], Phys. Rev. D **90**, 072003 (2014)

- [9] Q. T. Song, D. Y. Chen, X. Liu and T. Matsuki, Eur. Phys. J. C **75**, 30 (2015)
- [10] Z. G. Wang, Eur. Phys. J. C **75**, 25 (2015)
- [11] R. Aaij *et al.* [LHCb Collaboration], Phys. Rev. D **91**, 092002 (2015)
- [12] R. Aaij *et al.* [LHCb Collaboration], Phys. Rev. D **92**, 032002 (2015)
- [13] R. Aaij *et al.* [LHCb Collaboration], Phys. Rev. D **92**, 012012 (2015)
- [14] K. A. Olive *et al.* [Particle Data Group Collaboration], Chin. Phys. C **38**, 090001 (2014).
- [15] T. Latham *et al.*, <http://laura.hepforge.org/>
- [16] G. N. Fleming, Phys. Rev. **135**, B551 (1964).
- [17] D. Morgan, Phys. Rev. **166**, 1731 (1968).
- [18] D. Herndon, P. Soding and R. J. Cashmore, Phys. Rev. D **11**, 3165 (1975).
- [19] T. Latham and T. Gershon, J. Phys. G **36**, 025006 (2009)
- [20] J. Charles, A. Le Yaouanc, L. Oliver, O. Pene and J. C. Raynal, Phys. Lett. B **425**, 375 (1998)
- [21] I. J. R. Aitchison, Nucl. Phys. A **189**, 417 (1972).
- [22] S. U. Chung, J. Brose, R. Hackmann, E. Klempt, S. Spanier and C. Strassburger, Annalen Phys. **4**, 404 (1995).
- [23] T. Gershon, Phys. Rev. D **79**, 051301 (2009)
- [24] T. Gershon and M. Williams, Phys. Rev. D **80**, 092002 (2009)